OPTICS

Strong mode coupling-enabled hybrid photon-plasmon laser with a microfiber-coupled nanorod

Ning Zhou[1,2]†, Yuxin Yang[1]†, Xin Guo[1,3,4]†, Jue Gong[1], Zhangxing Shi[1], Zongyin Yang[5], Hao Wu[1], Yixiao Gao[1], Ni Yao[1], Wei Fang[1,3,4], Pan Wang[1,3,4]*, Limin Tong[1,6]*

Laser based on single plasmonic nanoparticle can provide optical frequency radiation far beyond the diffraction limit and is one of the ultimate goals of nanolasers, yet it remains a challenge to be realized because of the inherently high Ohmic loss. Here, we report the direct observation of lasing in microfiber-coupled single plasmonic nanoparticles enabled by strong mode coupling. We show that, by strongly coupling a gold nanorod (GNR) with the whispering gallery cavity of a dye-doped polymer microfiber (with diameter down to 2.0 μm), the substantially enhanced optical coherence of the hybrid photon-plasmon mode and effective gain accumulated from the active microfiber cavity enable single-mode laser emission from the GNR at room temperature with a threshold as low as 2.71 MW/cm^2 and a linewidth narrower than 2 nm.

INTRODUCTION

With the rapid developments in areas such as superresolution imaging, biochemical sensing, optical data storage, and on-chip optical interconnects, the demands for coherent sources that can provide optical frequency radiation below the diffraction limit in one or more spatial dimensions are ever-increasing in recent years. Plasmonic lasers (*1*), using surface plasmons in metallic nanostructures to achieve optical confinement and feedback, are an emerging coherent light source that can achieve a lasing cavity mode with feature size far beyond the diffraction limit and ultrafast modulation speed up to terahertz (*2*–*9*). Relying on various low-dimensional plasmonic nanostructures including metal films (*10*–*12*), nanowires (*13*), and particles (*14*–*16*), a number of plasmonic lasers have been successfully demonstrated by placing gain media in their optical near-field regions. Among them, metal nanoparticle-based lasers with the capability of extreme confinement of lasing modes, which is one of the ultimate goals of nanolasers (*2*), are of particular interest. However, up to date, almost all of the metal nanoparticle-based lasers are obtained in a cluster or an array of nanoparticles (*14*–*19*), laser based on single metal nanoparticles has not yet been convincingly realized. The difficulty in the realization of single nanoparticle–based plasmonic lasers lies in the high parasitic Ohmic loss associated with highly localized surface plasmon resonance (*20*), which requires unrealistically high gain difficult to be provided by gain media located in the optical near field of the resonant nanoparticle, not to mention the thermal damage induced by the high-density pump (*21*, *22*).

Here, by strong coupling a gold nanorod (GNR) with the whispering gallery cavity of an active polymer microfiber (Fig. 1), we report the direct observation of lasing in microfiber-coupled single plasmonic nanoparticles. The substantially enhanced coherence of the plasmonic resonance originating from the strong mode coupling between the GNR and the microfiber cavity (with diameters down to 2.0 μm), together with the accumulated gain from doped dyes in the microfiber cavity, enables single-mode laser emission from the GNR at room temperature with low threshold (~2.70 MW/cm^2) and narrow linewidth. The results demonstrated here provide a feasible approach for the realization of lasers based on single plasmonic nanoparticles and may find applications in areas such as ultraconfined field manipulation, ultrasensitive sensing, and on-chip optical interconnects.

RESULTS

Design of a microfiber-coupled single plasmonic nanorod laser

The configuration of our laser, enabled by strong mode coupling between a microfiber and a single plasmonic nanorod, is schematically illustrated in Fig. 1. A dye-doped polymethyl methacrylate (PMMA) microfiber with a diameter of several micrometers is used as the gain medium. To ensure high-quality whispering gallery mode (WGM) along its cross section (*23*), the microfiber is suspended across two glass substrates (Fig. 1A). By placing a GNR on the surface of the microfiber with its long axis perpendicular to the fiber length (Fig. 1B), a dominant hybrid photon-plasmon mode can be generated by strong coupling between the localized surface plasmon resonance (LSPR) mode of the GNR and WGM of the microfiber (*24*, *25*), which has a greatly reduced LSPR linewidth (i.e., enhanced coherence) and enhanced plasmonic fields around the nanorod, and is therefore beneficial for the realization of single nanoparticle–based lasers with acceptable threshold and narrow linewidth.

When the dye-doped microfiber is excited by a pump laser, a certain fraction of the photoluminescence (PL; i.e., dye emission) can be channeled into the hybrid mode as long as a good spectral overlap between the hybrid mode and the PL is satisfied. When the pump intensity is strong enough (e.g., population inversion within the whole hybrid cavity), the PL increases while recirculating back to the LSPR mode of the GNR within the WGM cavity (inset of Fig. 1B). Compared with previously reported nanoparticle-based

[1]State Key Laboratory of Modern Optical Instrumentation, College of Optical Science and Engineering, Zhejiang University, Hangzhou 310027, China. [2]School of Physics and Optoelectronic Engineering, Hangzhou Institute for Advanced Study, University of Chinese Academy of Sciences, Hangzhou 310024, China. [3]Jiaxing Key Laboratory of Photonic Sensing and Intelligent Imaging, Jiaxing 314000, China. [4]Intelligent Optics and Photonics Research Center, Jiaxing Institute Zhejiang University, Jiaxing 314000, China. [5]College of Information Science and Electronic Engineering, State Key Laboratory of Modern Optical Instrumentation, Zhejiang University, Hangzhou 310027, China. [6]Collaborative Innovation Center of Extreme Optics, Shanxi University, Taiyuan 030006, China.
*Corresponding author. Email: nanopan@zju.edu.cn (P.W.); phytong@zju.edu.cn (L.T.)
†These authors contributed equally to this work.

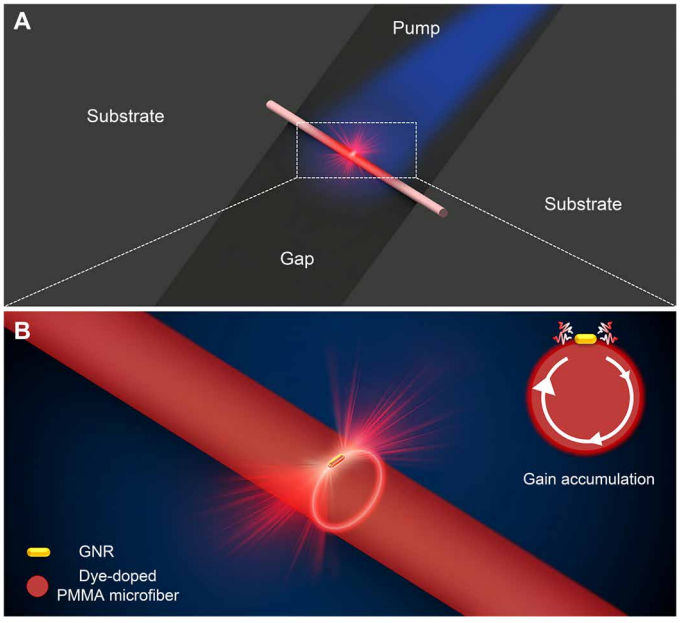

Fig. 1. Design of a microfiber-coupled single plasmonic nanorod laser. (**A**) Schematic illustration of a strong mode coupling-enabled hybrid photon-plasmon laser, realized by placing a GNR on the surface of a dye-doped polymethyl methacrylate (PMMA) microfiber suspended between two glass substrates. (**B**) Close-up view of the lasing structure. The inset is a schematic diagram showing gain accumulation.

lasing systems relying on local gain media, which can only acquire gain within a limited volume surrounding the nanoparticle (i.e., optical near field of the nanoparticle), the gain accumulation provided by the WGM cavity of the hybrid photon-plasmon system can offer a much higher accessible gain for compensating plasmonic loss. Therefore, together with the strong mode coupling-enabled linewidth narrowing, it is possible to break the current limitations to realize single plasmonic nanoparticle–based lasers with high performance.

Strong mode coupling-enabled linewidth narrowing

The strong mode coupling between LSPR mode of a GNR and WGM of a pure PMMA microfiber (i.e., passive microfiber) was first studied. Experimentally, GNRs were synthesized using a seed-mediated method (*26*). As shown in Fig. 2A, the sizes of GNRs are relatively uniform with average diameter and length of 38 and 84 nm, respectively. The longitudinal LSPR peak of a GNR deposited on a glass slide is around 630 nm, with a typical linewidth of about 49 nm (Fig. 2B). PMMA microfibers were fabricated by using a direct solution drawing technique (*27*). By immersing a microfiber into a small droplet of diluted nanorod solution (1 pM) and drying it in air, individual GNRs can be deposited on the surface of the microfiber. Figure 2C shows an optical microscope image of a suspended 2.5-μm-diameter PMMA microfiber with a GNR deposited on its surface, which can be visualized in the scanning electron microscope (SEM) image (Fig. 2D). The long axis of the GNR is perpendicular to the length of the microfiber, forming a photon-plasmon hybrid cavity (*24*, *25*, *28*, *29*). Under side illumination with a supercontinuum white light (fig. S1), a clear red scattering spot can be observed at the position of the GNR due to the excitation of the nanorod-microfiber coupled system (Fig. 2E). In contrast to the relatively broad linewidth of an uncoupled GNR (Fig. 2B), the linewidth of the dominant LSPR peak of the coupled GNR (Fig. 2F) is reduced down to ~8.0 nm (corresponding to a quality factor of ~82) along with a 7.5-fold enhancement in the peak intensity, resulting from the strong mode coupling (*24*, *25*). Simulated electric field distribution of an excited GNR on the surface of a 2.5-μm-diameter PMMA microfiber is presented in the inset of Fig. 2F, showing the coupling between LSPR mode of the GNR and WGM of the microfiber. Although the entire hybrid photon-plasmon cavity offers a relatively large mode volume, it is efficiently interfaced with free space via the tightly confined cavity mode on the GNR.

Microfiber-coupled single-nanorod hybrid photon-plasmon laser

The substantially improved quality factor of plasmonic resonance in a strongly coupled GNR makes it possible for realizing single nanoparticle–based hybrid photon-plasmon lasers with low threshold. Rhodamine 101 (R101), whose PL spectrum overlaps well with the LSPR mode of GNRs (fig. S2), was used as the gain medium and introduced into polymer microfibers by directly doping it into a PMMA solution before microfiber drawing (see Materials and Methods). To study the lasing action, single GNRs with its long axis perpendicular to the length of PMMA microfibers was first located by a dark-field scattering approach (see Materials and Methods), and then *s*-polarized (to minimize heating effect by avoiding the excitation of the transverse mode of GNRs) 532-nm laser pulses (4 ns in pulse width, 10 Hz in repetition rate; SLII-10, Continuum) were focused onto the nanorod region to excite the lasing structure at an oblique angle of 30° (Fig. 3A). The emission from the GNR was collected by a 100× objective [numerical aperture (NA) = 0.7] and then redirected to a spectrometer (Kymera 193i, Andor) for spectral analysis and a charge-coupled device (CCD) camera (DS-Fi3, Nikon) for imaging after passing through a 532-nm-wavelength notch filter to block the pump laser. After each measurement, the lasing structure was further characterized by SEM to characterize the size and position of the GNR, as well as the diameter of the microfiber. Under excitation with a pump density of 3.16 MW/cm^2, an evident luminous spot was observed (Fig. 3B) at the position of the GNR (with its long axis perpendicular to the length of the 2.4-μm-diameter microfiber for optimum coupling), while at other regions of the active microfiber, only relatively weak red fluorescence can be observed. Figure 3C shows typical pump density–dependent emission spectra collected from a lasing structure (constructed with a 2.5-μm-diameter active microfiber) around a GNR (with an aspect ratio of ~2.2). When the pump density was lower than 1.90 MW/cm^2, the emission spectrum from the coupled system is weak and flat, which originates from the spontaneous emission of the doped R101 dye. With the further increase of the pump density to 2.16, 2.45, and 2.78 MW/cm^2, a weak shoulder with a narrow linewidth appears at 623 nm, which subsequently increases sharply in the intensity with the increase of pump density to 3.16 and 3.59 MW/cm^2, showing clear evidence of single-mode lasing. The intensity of the lasing peak starts to decrease when the pump density is larger than 3.59 MW/cm^2, which is due to the photobleaching of the doped dyes under high pump density (e.g., the lasing emission lasts for about 60 s under a pump density of 2.78 MW/cm^2). The emission spectra can be well fitted with bi-Lorentzian curves (fig. S3) for the extraction of peak intensities of both the narrow lasing emission and broad R101 PL background. Figure 3D further gives the

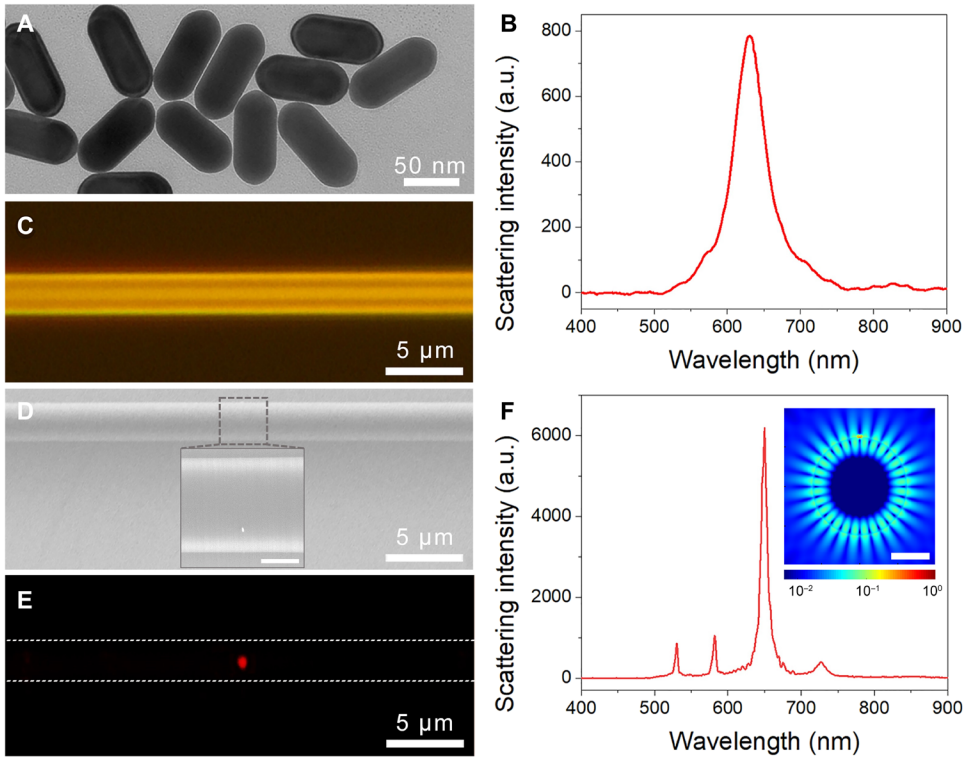

Fig. 2. Strong mode coupling-enabled linewidth narrowing. (**A**) Transmission electron microscopy image of GNRs. (**B**) Typical scattering spectrum of a GNR deposited on a glass slide. a.u., arbitrary units. (**C** to **E**) Bright-field optical microscopy (C), SEM (D), and dark-field scattering (E) images of a GNR-coupled PMMA microfiber (2.5 μm in diameter). The inset of (D) is an enlarged view of the nanorod region. Scale bar, 1 μm. The outline of the microfiber in (E) is indicated by white dashed lines. (**F**) Corresponding scattering spectrum of the microfiber coupled GNR shown in (E). Inset: Simulated modal profile of the coupled nanorod-microfiber system at the resonant wavelength of 646 nm. Scale bar, 1 μm.

pump density–dependent lasing emission peak intensity of the laser, showing a pronounced lasing threshold of about 2.71 MW/cm^2. Meanwhile, the linewidth of the emission is reduced from 2.90 to 1.53 nm when the pump density reaches the lasing threshold. In contrast, no lasing action was observed from the same microfiber at the area without any GNRs (Fig. 3, E and F). The emission spectra show an increase in the peak intensity around 616 nm and a moderate narrowing, which is mainly due to amplification by the optical feedback in the WGM cavity. The emission intensity decreases quickly with the further increase of the pump density due to the photobleaching of doped dyes. The absence of lasing action in the pure dye-doped microfiber is mainly due to the large bending loss of the WGMs in such a small cavity (*30*) that cannot be compensated by the gain in the dye-doped microfiber. Single-mode lasing from pure dye-doped PMMA microfibers can be observed when the microfiber diameter is increased to about 3.8 μm (figs. S4 and S5). These results further confirm that the measured lasing emission (Fig. 3C) comes from the microfiber-coupled GNR.

In addition, temporal coherence signature of the lasing action was investigated by measuring the second-order photon-correlation function via a Hanbury Brown–Twiss setup (see Materials and Methods and fig. S6), showing a typical lasing behavior of nanolasers around the lasing threshold (*19*, *31*–*35*): When the pump density is increased to approach the lasing threshold (fig. S7A), a clear thermal bunching of the photons can be observed with $g^2(0)$ larger than 1 (fig. S7B); when the pump density is further increased to exceed the threshold, the $g^2(0)$ value decreases to 1 along with a slight increase in the linewidth of $g^2(\tau)$ curve (fig. S7B), confirming the lasing action in the hybrid system (*31*, *32*, *34*). In contrast, no lasing behavior was observed from the same microfiber at the area without any GNRs (figs. S7, C and D).

The polarization property of the lasing emission from the hybrid photon-plasmon laser was also investigated by placing a linear polarizer before the spectrometer and CCD camera (Fig. 3A). As shown in Fig. 4A, for a lasing structure with the microfiber diameter of 2.5 μm, when the polarization of the polarizer is parallel to the long axis of the nanorod, the lasing output intensity is maximized. When the polarization of the polarizer is rotated to the direction perpendicular to the long axis of the nanorod, the output intensity is minimized. From the collected lasing spectra shown in Fig. 4C, a polarization ratio as high as 0.92 can be calculated for the lasing mode. Note that despite the similar diameter of microfibers used in lasing structures investigated in Figs. 3C and 4C, the peak wavelength of the lasing mode in Fig. 4C is red-shifted to around 658 nm. This is due to the increased aspect ratio of the GNR (~2.4; inset of Fig. 4C) that has a red-shifted LSPR peak. Therefore, this provides a simple and effective approach for tuning the laser wavelength. Despite the increase of bending loss of the WGM, lasing action can still be observed when the microfiber diameter is decreased down to 2.0 μm, as shown in Fig. 4 (D and F). The SEM image (Fig. 4E) convincingly demonstrates the existence of a GNR (aspect ratio of ~2.2) on the surface of a 2.0-μm-diameter microfiber with its orientation

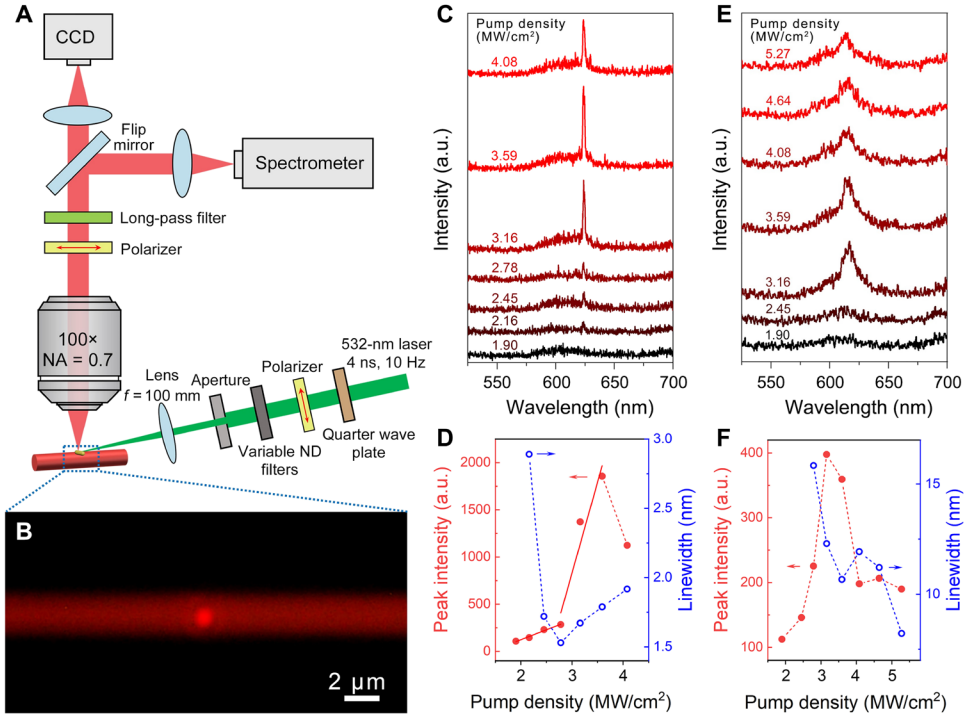

Fig. 3. Lasing characterization of the hybrid photon-plasmon laser. (**A**) Schematic illustration of the experimental setup. NA, numerical aperture; CCD, charge-coupled device. (**B**) Optical microscopy image of a lasing structure (constructed with a 2.4-μm-diameter active microfiber) under a pump power density of 3.16 MW/cm^2. (**C**) Pump density–dependent emission spectra collected around the GNR from another laser structure (constructed with a 2.5-μm-diameter active microfiber). (**D**) Corresponding pump density–dependent peak intensity and linewidth of the emissions. (**E**) Pump density–dependent emission spectra collected from the same microfiber at the area without any GNRs. (**F**) Corresponding pump density–dependent peak intensity and linewidth of the emissions.

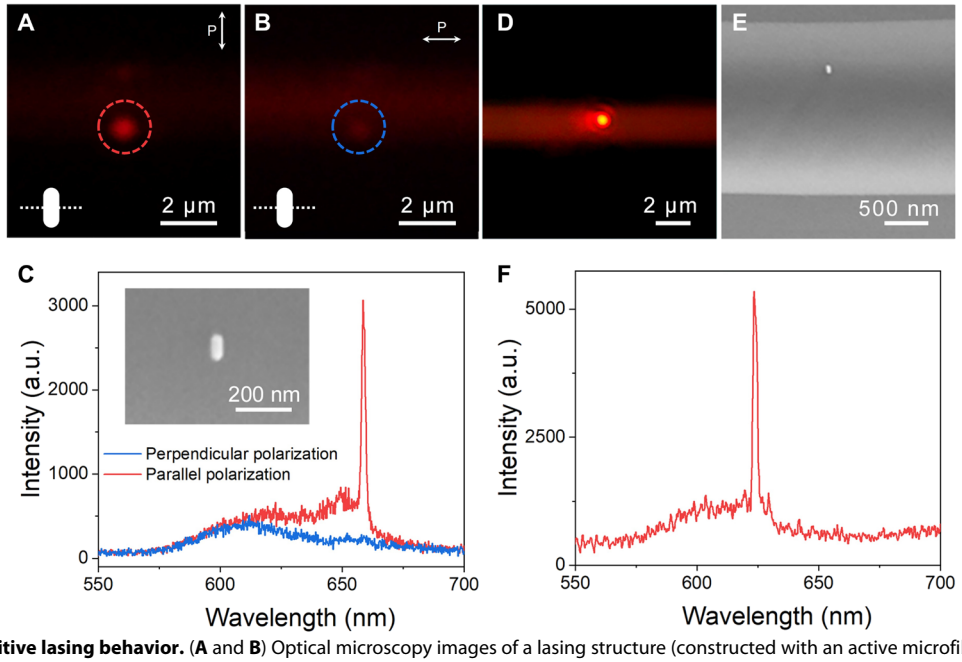

Fig. 4. Polarization-sensitive lasing behavior. (**A** and **B**) Optical microscopy images of a lasing structure (constructed with an active microfiber of 2.5 μm in diameter) taken at parallel and perpendicular polarizations (defined as the relative orientation between the polarization of the polarizer and the long axis of the nanrod), respectively, under a pump power density of 3.59 MW/cm^2. (**C**) Corresponding polarization-sensitive lasing spectra and SEM image of the lasing structure (inset). (**D**) Optical microscopy image of a lasing structure (constructed with an active microfiber of 2.0 μm in diameter) taken under a pump density of 3.59 MW/cm^2. (**E**) Corresponding SEM image of the lasing structure. (**F**) Corresponding spectrum of the lasing emission.

perpendicular to the fiber length. With the further decrease of the microfiber diameter, it is difficult to obtain lasing emission due to the marked increased bending loss of the WGMs (*30*).

DISCUSSION

In conclusion, we have demonstrated a microfiber-coupled nanorod laser at room temperature enabled by strong mode coupling. In addition to the use of active polymer microfibers as the cavity, it is also possible to exploit active microcavities of many other types, such as semiconductor nanowires with inherently high refractive index, high gain and optical stability (*25*, *36*, *37*), photonic crystal microcavities (*38*, *39*), microdisks (*40*), and dielectric photonic cavities with exotic states (*41*–*43*), for the construction of single nanoparticle–based lasers with improved stability and integrability. Meanwhile, the operation wavelength of single nanoparticle-based lasers can be readily tuned by using plasmonic nanoparticles with different materials and structural parameters (*14*, *44*–*47*). The single nanoparticle–based hybrid photon-plasmon lasers demonstrated here may open opportunities for manipulating ultraconfined coherent optical fields for applications including ultrasensitive sensing and superresolution imaging.

MATERIALS AND METHODS

Sample fabrication

PMMA microfibers used in the experiment were fabricated by physical drawing of solvated polymer. To prepare the polymer solution for passive microfibers, 1000 mg of PMMA powder [weight-average molecular weight (M_w) = 550,000; Alfa Aesar] was first dissolved in 5 ml of chloroform. Subsequently, 500 mg of epoxy resin (Araldite 506 from Sigma-Aldrich) was added into the solvated PMMA to reduce the viscosity, followed by magnetic stirring at room temperature for about 8 hours to ensure the homogeneous mixture. To prepare the polymer solution for active microfibers, in addition to the addition of PMMA and epoxy resin into 5 ml of chloroform with the same weights, 13 mg of R101 dye (from Exciton) was further added into the mixture solution and mixed well by magnetic stirring.

To fabricate PMMA microfibers, we used an electrochemically sharpened tungsten probe to physically dip up a bead out of the polymer solution onto a glass slide, withdrew the probe out of the polymer bead at a speed of about 0.5 m/s, and obtained microfibers after the evaporation of chloroform. To improve the quality of microfibers, all the fabrication process was conducted in a home-made glove box filled with abundant chloroform gas to decrease the evaporation rate of chloroform. The concentration of R101 dye in active microfibers is estimated to be ~20 mM.

Dark-field scattering setup

Scattering spectra of the coupled system were collected using a dark-field setup as shown in fig. S1. We used a beam of unpolarized white light (SC-5, Wuhan Yangtze Soton Laser Co. Ltd.) from a photonic crystal fiber to illuminate microfiber-coupled GNRs at an oblique angle of about 30° with respect to the microfiber axis. We used a 100× objective (NA = 0.7; CFI L plan BD ELWD, Nikon) to collect the scattered light, which was then redirected to a spectrometer (Kymera 193i, Andor) for spectral analysis and a CCD camera (DS-Fi3, Nikon) for imaging. A linear polarizer was inserted before the spectrometer and CCD camera to study the polarization property.

For the location of single GNRs (as well as the determination of GNRs' orientation) on active microfibers, a 640-nm laser (away from the absorption spectral range of the doped dye) was used as the illumination light source. GNRs with the orientation of their long axes perpendicular to the microfiber length (checked with a polarizer) were chosen for the following optical lasing characterization.

FDTD simulation

We have performed finite-difference time-domain (FDTD) simulations (Ansys Lumerical FDTD) on a hybrid nanorod-microfiber system. In the simulation, the nanorod was assumed to be 40 nm in diameter and 96 nm in length, and the microfiber was 2.5 μm in diameter. The dielectric constants of the GNR and the PMMA microfiber were adopted according to the fitting on the experimental data from Sultanova (*48*) and Johnson and Christy (*49*), respectively. For FDTD simulation, the investigated structure was excited with a polarized plane wave light. The mesh size was set as 3 nm, and the computational domain was terminated by the perfectly matched layer boundary.

Second-order correlation measurement

To conduct second-order correlation measurement on the hybrid photon-plasmon lasers, *s*-polarized 517-nm laser pulses (5 ps in pulse width stretched by multimode fiber, 25 kHz in repetition rate), generated from a 1034-nm femtosecond laser (500 fs; FemtoYL, Wuhan Yangtze Soton Laser Co. Ltd.) by frequency doubling and pulse broadening, were used as the pump source. As shown in fig. S7A, the emission collected from the GNR was first equally split with a beamsplitter into two parts. The reflected part was sent into a spectrometer (QE Pro, Ocean Insight Inc.) (after passing through a 620-nm-wavelength long-pass filter) for spectral analysis, and the transmitted part was used for second-order correlation analysis. After passing through a monochromator (SP2150, Teledyne Princeton Instruments) to filter out narrowband (~10 nm) emission signal around the lasing peak, the output signal was equally split and then detected by a pair of single-photon detectors operated in the photon counting mode. The timing jitter of the exciting pulses was calibrated through the reference photon detector.

SUPPLEMENTARY MATERIALS

Supplementary material for this article is available at https://science.org/doi/10.1126/sciadv.abn2026

REFERENCES AND NOTES

1. D. J. Bergman, M. I. Stockman, Surface plasmon amplification by stimulated emission of radiation: Quantum generation of coherent surface plasmons in nanosystems. *Phys. Rev. Lett.* **90**, 27402 (2003).
2. P. Norvig, D. A. Relman, D. B. Goldstein, D. M. Kammen, D. R. Weinberger, L. C. Aiello, G. Church, J. L. Hennessy, J. Sachs, A. Burrows, G. P. Pisano, J. R. Goldstein, P. Anastas, R. Klausner, D. Baltimore, D. R. Montgomery, T. M. Baer, N. P. Bigelow, R. D. Holt, J. K. Nicholson, 2020 visions. *Nature* **463**, 26–32 (2010).
3. R.-M. Ma, R. F. Oulton, V. J. Sorger, X. Zhang, Plasmon lasers: Coherent light source at molecular scales. *Laser Photonics Rev.* **7**, 1–21 (2012).
4. Y. Yin, T. Qiu, J. Li, P. K. Chu, Plasmonic nano-lasers. *Nano Energy* **1**, 25–41 (2012).
5. P. Berini, I. De Leon, Surface plasmon-polariton amplifiers and lasers. *Nat. Photon.* **6**, 16–24 (2012).
6. R.-M. Ma, R. F. Oulton, Applications of nanolasers. *Nat. Nanotech.* **14**, 12–22 (2019).
7. H. Wu, Y. Gao, P. Xu, X. Guo, P. Wang, D. Dai, L. Tong, Plasmonic nanolasers: Pursuing extreme lasing conditions on nanoscale. *Adv. Opt. Mater.* **7**, 1900334 (2019).
8. M. I. Stockman, Brief history of spaser from conception to the future. *Adv. Photonics* **2**, 054002 (2020).
9. S. I. Azzam, A. V. Kildishev, R.-M. Ma, C.-Z. Ning, R. Oulton, V. M. Shalaev, M. I. Stockman, J.-L. Xu, X. Zhang, Ten years of spasers and plasmonic nanolasers. *Light Sci. Appl.* **9**, 90 (2020).

10. R. F. Oulton, V. J. Sorger, T. Zentgraf, R.-M. Ma, C. Gladden, L. Dai, G. Bartal, X. Zhang, Plasmon lasers at deep subwavelength scale. *Nature* **461**, 629–632 (2009).
11. R.-M. Ma, R. F. Oulton, V. J. Sorger, G. Bartal, X. Zhang, Room-temperature sub-diffraction-limited plasmon laser by total internal reflection. *Nat. Mater.* **10**, 110–113 (2011).
12. Y.-J. Lu, J. Kim, H.-Y. Chen, C. Wu, N. Dabidian, C. E. Sanders, C.-Y. Wang, M.-Y. Lu, B.-H. Li, X. Qiu, W.-H. Chang, L.-J. Chen, G. Shvets, C.-K. Shih, S. Gwo, Plasmonic nanolaser using epitaxially grown silver film. *Science* **337**, 450–453 (2012).
13. X. Wu, Y. Xiao, C. Meng, X. Zhang, S. Yu, Y. Wang, C. Yang, X. Guo, C. Z. Ning, L. Tong, Hybrid photon-plasmon nanowire lasers. *Nano Lett.* **13**, 5654–5659 (2013).
14. J. Y. Suh, C. H. Kim, W. Zhou, M. D. Huntington, D. T. Co, M. R. Wasielewski, T. W. Odom, Plasmonic bowtie nanolaser arrays. *Nano Lett.* **12**, 5769–5774 (2012).
15. W. Zhou, M. Dridi, J. Y. Suh, C. H. Kim, D. T. Co, M. R. Wasielewski, G. C. Schatz, T. W. Odom, Lasing action in strongly coupled plasmonic nanocavity arrays. *Nat. Nanotech.* **8**, 506–511 (2013).
16. M. Ramezani, A. Halpin, A. I. Fernández-Domínguez, J. Feist, S. R.-K. Rodriguez, F. J. Garcia-Vidal, J. G. Rivas, Plasmon-exciton-polariton lasing. *Optica* **4**, 31–37 (2017).
17. A. Yang, T. B. Hoang, M. Dridi, C. Deeb, M. H. Mikkelsen, G. C. Schatz, T. W. Odom, Real-time tunable lasing from plasmonic nanocavity arrays. *Nat. Commun.* **6**, 6939 (2015).
18. T. K. Hakala, H. T. Rekola, A. I. Väkeväinen, J.-P. Martikainen, M. Nečada, A. J. Moilanen, P. Törmä, Lasing in dark and bright modes of a finite-sized plasmonic lattice. *Nat. Commun.* **8**, 13687 (2017).
19. A. Fernandez-Bravo, D. Wang, E. S. Barnard, A. Teitelboim, C. Tajon, J. Guan, G. C. Schatz, B. E. Cohen, E. M. Chan, P. J. Schuck, T. W. Odom, Ultralow-threshold, continuous-wave upconverting lasing from subwavelength plasmons. *Nat. Mater.* **18**, 1172–1176 (2019).
20. F. Wang, Y. R. Shen, General properties of local plasmons in metal nanostructures. *Phys. Rev. Lett.* **97**, 206806 (2006).
21. G. Kewes, K. Herrmann, R. Rodríguez-Oliveros, A. Kuhlicke, O. Benson, K. Busch, Limitations of particle-based spasers. *Phys. Rev. Lett.* **118**, 237402 (2017).
22. Y. Gao, H. Wu, N. Zhou, Y. Yang, X. Guo, P. Wang, J. You, Y. Gu, G. Lu, Q. Gong, L. Tong, Single-nanorod plasmon nanolaser: A route toward a three-dimensional ultraconfined lasing mode. *Phys. Rev. A* **102**, 63520 (2020).
23. M. Sumetsky, Mode localization and the Q-factor of a cylindrical microresonator. *Opt. Lett.* **35**, 2385–2387 (2010).
24. P. Wang, Y. Wang, Z. Yang, X. Guo, X. Lin, X.-C. Yu, Y.-F. Xiao, W. Fang, L. Zhang, G. Lu, Q. Gong, L. Tong, Single-band 2-nm-line-width plasmon resonance in a strongly coupled Au nanorod. *Nano Lett.* **15**, 7581–7586 (2015).
25. Y. Jin, L. Yang, C. Pan, Z. Shi, B. Cui, P. Xu, Y. Yang, N. Zhou, X. Guo, P. Wang, L. Tong, Strong coupling of a plasmonic nanoparticle to a semiconductor nanowire. *Nanophotonics* **10**, 2875–2881 (2021).
26. B. Nikoobakht, M. A. El-Sayed, Preparation and growth mechanism of gold nanorods (NRs) using seed-mediated growth method. *Chem. Mater.* **15**, 1957–1962 (2003).
27. P. Wang, L. Zhang, Y. Xia, L. Tong, X. Xu, Y. Ying, Polymer nanofibers embedded with aligned gold nanorods: A new platform for plasmonic studies and optical sensing. *Nano Lett.* **12**, 3145–3150 (2012).
28. F. Gu, L. Zhang, Y. Zhu, H. Zeng, Free-space coupling of nanoantennas and whispering-gallery microcavities with narrowed linewidth and enhanced sensitivity. *Laser Photonics Rev.* **9**, 682–688 (2015).
29. Q. Ai, L. L. Gui, D. Paone, B. Metzger, M. Mayer, K. Weber, A. Fery, H. Giessen, Ultranarrow second-harmonic resonances in hybrid plasmon-fiber cavities. *Nano Lett.* **18**, 5576–5582 (2018).
30. L. He, Ş. K. Özdemir, L. Yang, Whispering gallery microcavity lasers. *Laser Photonics Rev.* **7**, 60–82 (2013).
31. S. H. Pan, Q. Gu, A. El Amili, F. Vallini, Y. Fainman, Dynamic hysteresis in a coherent high-β nanolaser. *Optica* **3**, 1260–1265 (2016).
32. B. Mayer, L. Janker, B. Loitsch, J. Treu, T. Kostenbader, S. Lichtmannecker, T. Reichert, S. Morkötter, M. Kaniber, G. Abstreiter, C. Gies, G. Koblmüller, J. J. Finley, Monolithically integrated high-β nanowire lasers on silicon. *Nano Lett.* **16**, 152–156 (2016).
33. W. E. Hayenga, H. Garcia-Gracia, H. Hodaei, C. Reimer, R. Morandotti, P. Likamwa, M. Khajavikhan, Second-order coherence properties of metallic nanolasers. *Optica* **3**, 1187–1193 (2016).
34. S. H. Pan, S. S. Deka, A. El Amili, Q. Gu, Y. Fainman, Nanolasers: Second-order intensity correlation, direct modulation and electromagnetic isolation in array architectures. *Prog. Quant. Electron.* **59**, 1–18 (2018).
35. Y.-H. Hsieh, B.-W. Hsu, K.-N. Peng, K.-W. Lee, C. W. Chu, S.-W. Chang, H.-W. Lin, T.-J. Yen, Y.-J. Lu, Perovskite quantum dot lasing in a gap-plasmon nanocavity with ultralow threshold. *ACS Nano* **14**, 11670–11676 (2020).
36. F. Gu, Z. Yang, H. Yu, J. Xu, P. Wang, L. Tong, A. Pan, Spatial bandgap engineering along single alloy nanowires. *J. Am. Chem. Soc.* **133**, 2037–2039 (2011).
37. S. W. Eaton, A. Fu, A. B. Wong, C.-Z. Ning, P. Yang, Semiconductor nanowire lasers. *Nat. Rev. Mater.* **1**, 16028 (2016).
38. S. Wu, S. Buckley, J. R. Schaibley, L. Feng, J. Yan, D. G. Mandrus, F. Hatami, W. Yao, J. Vučković, A. Majumdar, X. Xu, Monolayer semiconductor nanocavity lasers with ultralow thresholds. *Nature* **520**, 69–72 (2015).
39. Y. Li, J. Zhang, D. Huang, H. Sun, F. Fan, J. Feng, Z. Wang, C. Z. Ning, Room-temperature continuous-wave lasing from monolayer molybdenum ditelluride integrated with a silicon nanobeam cavity. *Nat. Nanotechnol.* **12**, 987–992 (2017).
40. Y. Ye, Z. J. Wong, X. Lu, X. Ni, H. Zhu, X. Chen, Y. Wang, X. Zhang, Monolayer excitonic laser. *Nat. Photon.* **9**, 733–737 (2015).
41. K. Koshelev, G. Favraud, A. Bogdanov, Y. Kivshar, A. Fratalocchi, Nonradiating photonics with resonant dielectric nanostructures. *Nanophotonics* **8**, 725–745 (2019).
42. M. A. Miri, A. Alù, Exceptional points in optics and photonics. *Science* **363**, eaar7709 (2019).
43. A. S. Solntsev, G. S. Agarwal, Y. S. Kivshar, Metasurfaces for quantum photonics. *Nat. Photonics* **15**, 327–336 (2021).
44. H. Chen, L. Shao, Q. Li, J. Wang, Gold nanorods and their plasmonic properties. *Chem. Soc. Rev.* **42**, 2679–2724 (2013).
45. B. Doiron, M. Mota, M. P. Wells, R. Bower, A. Mihai, Y. Li, L. F. Cohen, N. M. Alford, P. K. Petrov, R. F. Oulton, S. A. Maier, Quantifying figures of merit for localized surface plasmon resonance applications: A materials survey. *ACS Photonics* **6**, 240–259 (2019).
46. K. G. Cognée, H. M. Doeleman, P. Lalanne, A. F. Koenderink, Cooperative interactions between nano-antennas in a high-Q cavity for unidirectional light sources. *Light Sci. Appl.* **8**, 115 (2019).
47. I. M. Palstra, H. M. Doeleman, A. F. Koenderink, Hybrid cavity-antenna systems for quantum optics outside the cryostat? *Nanophotonics* **8**, 1513–1531 (2019).
48. N. Sultanova, S. Kasarova, I. Nikolov, Dispersion properties of optical polymers. *Acta Phys. Pol.* **116**, 585–587 (2009).
49. P. B. Johnson, R. W. Christy, Optical constants of the noble metals. *Phys. Rev. B.* **6**, 4370–4379 (1972).

Acknowledgments

Funding: This work was supported by the National Natural Science Foundation of China (61635009, 62075195, 12004333, and 62005236), the National Key Research and Development Project of China (2018YFB2200400), the Natural Science Foundation of Zhejiang Province (LR21F050002), and the Fundamental Research Funds for the Central Universities. **Author contributions:** L.T., X.G., and P.W. conceived and designed the experiments. N.Z., Y.Y., and X.G. prepared the samples, performed the optical measurements, and analyzed the data. J.G., Y. Y., and N.Z. conducted the second-order correlation measurement under the supervision of W.F. N.Z., Y.Y., X.G., P.W., and L.T. prepared the manuscript. All the authors discussed the results and contributed to the manuscript. **Competing interests:** The authors declare that they have no competing interests. **Data and materials availability:** All data needed to evaluate the conclusions in the paper are present in the paper and/or the Supplementary Materials.

Submitted 11 November 2021
Accepted 23 May 2022
Published 8 July 2022
10.1126/sciadv.abn2026